AIAA JOURNAL
Vol. 44, No. 6, June 2006

# Comparison of Strategies for the Active Control of Buzz-Saw Tones

M. J. Wilkinson* and P. F. Joseph†
*University of Southampton, Southampton, England SO17 1BJ, United Kingdom*

**The results are presented of a feasibility study into the use of active control to reduce the low-engine-order components of buzz-saw noise produced in an aeroengine. It is shown that effective control performance can be achieved using a single ring of circumferentially spaced control actuators and a single ring of error sensors. Two control approaches are investigated: the minimization of the sum of the squared pressures at the error sensors, and the minimization of the sum of weighted squared spinning mode amplitudes. A comparison is made between the performance obtained by these control objectives. It is shown that pressure minimization and minimization of spinning mode amplitudes at the duct walls yields identical control performance. It is also shown that the amplitude of the evanescent modes excited by the control actuators is the fundamental factor in limiting control performance when noise and extraneous modes are absent at the error sensors. The variation of sound power reduction vs tip speed is investigated in detail. It is shown that, following control, a new set of resonances arise because of standing waves set up between the secondary sources and the duct exhaust termination and between the sensors and the duct inlet termination. Considerable improvements in control performance can be achieved by weighting the modal control objective such that control is focussed on the buzz-saw mode.**

## Nomenclature

| | | |
|---|---|---|
| $a$ | = | duct radius |
| $a_{m,n}$ | = | modal amplitude |
| $\hat{a}_m$ | = | spinning mode amplitude at the duct wall |
| $\hat{\boldsymbol{a}}_m$ | = | vector of spinning mode amplitudes |
| $a_{p0}$ | = | amplitude of the buzz-saw mode forward of the fan plane |
| $\boldsymbol{B}$ | = | matrix of the complex modal transfer impedances |
| $c_0$ | = | speed of sound |
| $J_m$ | = | Bessel function |
| $k$ | = | acoustic wave number |
| $k_r$ | = | radial component of the acoustic wave number |
| $M_t$ | = | tip-speed Mach number |
| $M_x$ | = | axial-flow Mach number |
| $m$ | = | azimuthal mode order |
| $m_B$ | = | spinning mode order of the buzz-saw mode |
| $N_{m,n}$ | = | normalization constant |
| $n$ | = | radial mode order |
| $\boldsymbol{p}$ | = | vector of pressures measured at the error sensors |
| $\boldsymbol{p}_p$ | = | vector of pressure caused by the primary source |
| $\boldsymbol{p}_s$ | = | vector of pressure caused by the secondary sources |
| $Q_m$ | = | modal source strength |
| $q$ | = | volumes velocity of the source |
| $\boldsymbol{q}_s$ | = | vector of complex secondary source strengths |
| $R^{\pm}_{m,n}$ | = | modal reflection coefficients |
| $r$ | = | radial position of the error sensor |
| $\boldsymbol{W}$ | = | matrix of modal weighting coefficients |
| $w_m$ | = | modal weighting coefficient |
| $x_e$ | = | axial position of the error sensor array |
| $x_f$ | = | axial position of the fan |
| $\boldsymbol{Z}$ | = | matrix of complex transfer impedances |
| $\alpha$ | = | $\sqrt{(1-\zeta_{m,n})}$ |
| $\beta_{m,n}$ | = | modal admittances |
| $\gamma_{m,n}$ | = | power function |
| $\zeta_{m,n}$ | = | cutoff ratio |
| $\theta$ | = | azimuthal position of the error sensor |
| $\rho$ | = | density |
| $\phi^{\pm}_{m,n}$ | = | complex reflectivity factors |
| $\Psi_{m,n}$ | = | radial mode shape function |
| $\psi_{m,n}$ | = | mode shape function |

Presented as Paper 2004-2850 at the AIAA/CEAS 10th Aeroacoustics Conference, Manchester, England, United Kingdom, 10–12 May 2004; received 18 February 2005; revision received 2 December 2005; accepted for publication 9 December 2005. 

*Research Assistant, Institute of Sound and Vibration Research.
†Senior Lecturer in Acoustics, Institute of Sound and Vibration Research. Member AIAA.

## I. Introduction

BUZZ-SAW noise is produced in a turbofan engine at takeoff and occurs when the fan tip speed becomes supersonic. It comprises a number of tones at multiples of the shaft rotational frequency. (Hence, buzz-saw noise is sometimes referred to as multiple pure tone noise.) Currently, passive acoustic liner sections are used in engine nacelles in order to attenuate this sound field. However, these liners do not have sufficient thickness to attenuate the very low-engine-order components of buzz-saw noise. It is therefore proposed that an active noise control system be used in conjunction with the liner section to further attenuate the buzz-saw noise field. However, in this paper it shall be assumed that the liner section in practice has no effect on the sound field other than to reduce the levels of the buzz-saw noise at the error sensors such that they can be asssumed to propagate linearly along the duct. However, even in the absence of the liner there is strong evidence to suggest that low-engine-order (EO) tones propagate linearly along the duct. McAlpine et al.[1] has demonstrated, by experiment and by computer simulation, that modification of the mode amplitudes through nonlinear interaction between the different EO and through energy dissipation by the shocks is generally weak for the low engine order tones (Fig. 2 of McAlpine et al.[1]). Moreover, the levels of the tones of engine order of less than about 10 appear to be typically 20–30 dB lower than the level of the higher engine orders (Fig. 9 of McAlpine et al.[1]). By contrast, tones at higher engine orders are strongly affected by these nonlinear mechanisms.

The use of nacelle-mounted active control systems has been the subject of much research over the past 15 years.[2–7] However, this research has focused almost exclusively on the attenuation of rotor-stator interaction tones produced by the interaction of the rotor wake with the stator vanes and occur at harmonics of the blade passing frequency (BPF) of the fan. At the high frequencies associated with BPF, a large number of sources and sensors are required for effective control.[8] This is largely to prevent spillover into the potentially

large number of modes that can propagate at these high frequencies. However, the low-frequency tonal components of buzz-saw noise occur at much lower frequencies, and hence fewer modes can propagate in the duct, thereby requiring fewer sources and and sensors to control the sound field. The number of sources and sensors needed for effective control of buzz-saw noise was discussed in a preliminary study by the authors.[9] However, we shall show in Sec. IV that the presence of cutoff modes is the factor that fundamentally limits active control performance in the hypothetical situation when no noise or extraneous modes are present.

Buzz-saw tones occur at harmonics (EO) of the shaft rotational frequency. At a single EO, the buzz-saw tone is dominated by a single propagating azimuthal mode order $m = m_B = \text{EO}$. Moreover, except at higher EO, only the first radial order $n = 1$ is usually cut on. This means that at each EO only a single dominant mode needs to be controlled, which can be achieved using a single ring of sources and sensors with no possibility of spillover into higher order radial mode order because these are cut off.

A quantity of importance in duct acoustics is the modal cutoff ratio $\zeta_{m,n}$. Modes of similar cutoff ratio have similar transmission and radiation characteristics. Modes with $\zeta_{m,n}$ values close to zero are well cutoff, with the cutoff frequency corresponding to $\zeta_{m,n} = 1$. The cutoff ratio $\zeta_{m,n}$ for the $(m, n)$th mode at a nondimensional frequency $ka$ can be written as

$$\zeta_{m,n} = \frac{ka}{k_{r_{m,n}} a\left(1 - M_x^2\right)^{\frac{1}{2}}} = \frac{mM_t}{k_{r_{m,n}} a\left(1 - M_x^2\right)^{\frac{1}{2}}} \tag{1}$$

where $k$ is the acoustic wave number $\omega/c$, $k_{r_{m,n}}$ is the radial component of the wave number of the $(m, n)$th mode, $m$ is the spinning mode order, and $M_t$ is the tip speed Mach number of the rotor. To a good approximation, $k_{r_{m,n}} a \approx m + 1$; therefore, Eq. (1) suggests that the cutoff ratios of the buzz-saw modes at different frequencies are very similar in magnitude and are usually close to one and hence are only just cut on. Modes close to cut off are strongly reflected by the duct terminations, leading to strong axial standing waves within the inlet duct. The effect of standing waves on control performance will be studied in detail in Sec. IV.

The following section describes further the modal structure of the buzz-saw noise field. A finite-length duct model, which is later used for predicting active control performance, is now described.

## II. Model of the Buzz-Saw Sound Field in the Engine Duct

Figure 1 shows a schematic representation of the finite-length duct model and the axial positions of the actuator ring $x_s$, sensor ring $x_e$, and fan $x_f$ used in the computer simulations.

The following assumptions are made in the model:

1) The engine inlet is a finite-length, axisymmetric circular duct with rigid walls containing an axial, uniform mean flow.

2) The modal amplitudes of the primary field in the absence of reflections in the duct (the sound field generated by the buzz-saw noise) are known at the fan plane $x_f$.

3) The secondary sources are mounted flush with the duct wall and behave as point monopoles.

4) At tip speeds close to $M_t = 1$, the buzz-saw tone associated with each EO generates a single propagating primary mode $m = m_B = \text{EO}$,[10] which propagates linearly along the duct.

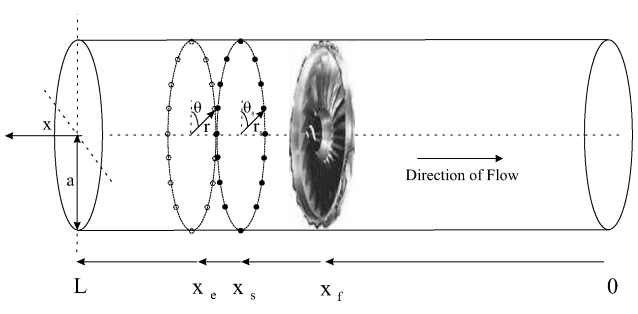


**Fig. 1 Schematic diagram of the duct model.**

5) Blockage of the sound field by the rotor and stator can be neglected.

The theory used to describe the sound field in the finite duct model is developed from that presented by Morfey[11] for a finite-length duct with axial uniform mean flow. The expression for the acoustic pressure in the duct excited by a point secondary source at $(x_s, r, \theta_s)$ with volume velocity $q(x_s, r_s, \theta_s)$ at a single error sensor position $(x_e, r, \theta)$ in a medium of density $\rho$ and sound speed $c_0$ is given by

$$p_s(x_e, r, \theta) = \sum_{m=-\infty}^{\infty} \sum_{n=1}^{\infty} \frac{i\rho c_0 q(x_s, r_s, \theta_s)\psi_{m,n}(r, \theta)\psi^*_{m,n}(r_s, \theta_s)}{S\alpha_{m,n}\left[\tan \phi^+_{m,n}(x_s) - \tan \phi^-_{m,n}(x_s)\right]}$$

$$\times \frac{\cos \phi^+_{m,n}(x_e)}{\cos \phi^+_{m,n}(x_s)} \exp\left[\frac{-iM_x k(x_e - x_s)}{1 - M_x^2}\right] \tag{2}$$

where $\psi_{m,n}(r, \theta)$ is the normalized shape function of the mode $(m, n)$ given by

$$\psi_{m,n}(r, \theta) = \frac{J_m\left(k_{r_{m,n}} r\right) e^{im\theta}}{N_{m,n}} = \Psi_{m,n}(r) e^{im\theta} \tag{3}$$

where $N_{m,n}$ is a constant chosen such that the shape functions satisfy the normalization condition $S^{-1} \int_S |\psi_{m,n}|^2 \, \mathrm{d}S = 1$, where $S$ is the duct cross-sectional area.

The terms $\phi^{\pm}_{m,n}$ are complex reflectivity phase factors defined in Eq. (4) and (5).[11] These are defined from the complex modal reflection coefficients at the duct terminations $R^+_{m,n} = \exp\{2i[\phi^+_0 - \alpha_{m,n} kL/(1 - M_x^2)]\}$ at the inlet and $R^-_{m,n} = \exp[2i(\phi^-_0)]$ at the exhaust. The terms $\phi^{\pm}_0$ are the complex reflection phase factors assuming that each termination is at $x = 0$:

$$\phi^+_{m,n}(x) = \frac{\ell_n R^+_{m,n}}{2i} + \frac{\alpha_{m,n} k(L - x)}{1 - M_x^2} \tag{4}$$

$$\phi^-_{m,n}(x) = \frac{-\ell_n R^-_{m,n}}{2i} + \frac{\alpha_{m,n} k(-x)}{1 - M_x^2} \tag{5}$$

An expression similar to Eq. (2) describes the pressure in the duct caused by the buzz-saw mode $m_B$ with amplitude $a_{p_0}$ at the fan plane in the absence of reflections.[12] This expression differs from Eq. (2) because the buzz-saw mode is only transmitted initially in the direction forward of the fan but is then repeatedly reflected between the inlet and exhaust terminations. This occurs because the relative flow behind the fan is generally subsonic, and thus shock waves cannot propagate.[13] At a single EO, for which only the single spinning mode $m_B = \text{EO}$ is present, the primary sound field can be written as[12]

$$p_p(x_e, r, \theta) = \sum_{n=1}^{\infty} \frac{a_{p_0}\psi_{m_B,n}(r, \theta) i e^{i\phi^-_{m_B,n}(x_f)}}{[\tan \phi^+_{m_B,n}(x_f) - \tan \phi^-_{m_B,n}(x_f)]}$$

$$\times \frac{\cos \phi^+_{m_B,n}(x_e)}{\cos \phi^+_{m_B,n}(x_f)} \exp\left[\frac{-iM_x k(x_e - x_f)}{1 - M_x^2}\right] \tag{6}$$

In the preceding equations, the parameter $\alpha_{m,n}$ is the ratio of the axial component of the wavenumber $k_{x_{m,n}}$ to the acoustic wave number $k$, taking a value of zero at cut off and tending to one well above cut off. It is related to $\zeta_{m,n}$ by the expression

$$\alpha_{m,n} = \sqrt{1 - \zeta_{m,n}} \tag{7}$$

The reflection coefficients $R^{\pm}_{m,n}$ at the inlet and exhaust terminations were calculated using Zorumski's generalized impedance method for the modal reflection coefficients for a semi-infinite duct in the absence of flow, terminated by an infinite, rigid baffle.[14] By applying the coordinate transformation suggested by Johnston and Ogimoto, the theory was modified to include a uniform mean flow.[15] The resulting reflection coefficients were shown to be energy conserving when the definition of acoustic energy in flow defined by

Morfey[11] is used. The modulus of the modal reflection coefficient is equal to one at the mode cutoff frequency $\zeta = 1$ for all values of the axial flow Mach number $M_x$. As buzz-saw modes are characteristically close to cutoff, as explained in Sec. I, strong axial resonances are a feature of the in-duct buzz-saw noise field. The effect of modal reflectivity on control performance will be assessed in Sec. IV.

Note that blockage by the rotor and stator also introduces standing waves in the engine; these will not be considered here.

## III. Active Control Strategies

### A. Pressure Minimization

The simplest practical approach consists of the minimization of the sum of the square pressures at an array of error sensors. This is the simplest strategy to implement as it does not require any phase calibration of the error sensors, which is necessary when implementing, for example, modal control techniques. The control performance of a modal control strategy will be discussed in Sec. III.B.

In the case of pressure minimization, the cost function we seek to minimize can be written in vector form as $J = \boldsymbol{p}^H \boldsymbol{p}$, where $\boldsymbol{p}$ is the vector of pressures at the error sensors and can be expressed as the sum of contributions from the primary field $\boldsymbol{p}_p$ and the secondary field $\boldsymbol{p}_s$. The vector of primary sound field pressures $\boldsymbol{p}_p$ can be calculated using Eq. (6). The vector of secondary field pressures $\boldsymbol{p}_s$ can be expressed as the vector product of a matrix of complex transfer impedances $\boldsymbol{Z}$ between the sources and sensors and a vector of the complex source strengths $\boldsymbol{q}_s$. Optimum values for the secondary source strength vector that minimizes $J$ can be determined from

$$\boldsymbol{q}_{\text{opt}} = -[\boldsymbol{Z}^H \boldsymbol{Z}]^{-1} \boldsymbol{Z}^H \boldsymbol{p}_p \tag{8}$$

### B. Modal Control

An alternative to pressure minimization is to minimize the modal amplitudes. The sound power is reduced to zero by driving the mode amplitudes to zero. This approach requires a complete modal decomposition of the sound field, which requires the use of many sensors and a high computational overhead to perform this decomposition in real time. We shall consider a more pragmatic approach and investigate the control performance obtained by minimizing the sum of weighted square spinning mode amplitudes of the sound field at the duct wall evaluated by a single ring of sensors. The cost function in this case can be written as

$$J = \sum_{m=-\infty}^{\infty} |w_m \hat{a}_m|^2 = \hat{\boldsymbol{a}}_m^H \boldsymbol{W} \hat{\boldsymbol{a}}_m \tag{9}$$

where $\hat{\boldsymbol{a}}_m$ is a vector of the spinning mode amplitudes at the duct wall, which can be written as the sum of the primary and secondary spinning mode amplitudes $\hat{\boldsymbol{a}}_{m_p}$ and $\hat{\boldsymbol{a}}_{m_s}$, respectively. These can be determined by performing a modal decomposition of the pressure measurements at the error sensors.

The matrix $\boldsymbol{W}$ is a diagonal matrix that can be used to weight the cost function such that control is focused only on certain spinning mode orders.

The optimum source strength vector can be found as before, where the matrix $\boldsymbol{B}$ is now the complex modal transfer impedances between the sources and sensors, such that the optimum source strength vector is given by

$$\boldsymbol{q}_{\text{opt}} = -[\boldsymbol{B}^H \boldsymbol{B}]^{-1} \boldsymbol{B}^H \hat{\boldsymbol{a}}_{m_p} \tag{10}$$

In this paper, active control performance will be quantified from the reduction in sound power after control. The sound power upstream of the error sensor array (duct inlet) is deduced from the sum of the modal power components $W = \sum_{m,n} W_{m,n}(x)$, where[11]

$$W_{m,n}(x) = \gamma_{m,n}(x) |a_{m,n}(x)|^2 \tag{11}$$

$$\gamma_{m,n}(x) = S/2\rho c_0 \left\{ \left(1 + M_x^2\right) \text{Re}\{\beta_{m,n}(x)\} + M_x \left[1 + |\beta_{m,n}(x)|^2\right] \right\} \tag{12}$$

where $a_{m,n}$ is the mode amplitude, such that $p_{m,n}(x, r, \theta) = a_{m,n}(x) \psi_{m,n}(r, \theta)$ and $\beta_{m,n}$ is the modal admittance defined as the ratio of the modal axial velocity $u_{m,n}$ to the pressure $p_{m,n}$, given by[11]

$$\beta_{m,n}(x) = \rho c_0 \frac{u_{m,n}(x)}{p_{m,n}(x)} = \frac{-i\alpha_{m,n}\left(1 - M_x^2\right) \tan \phi_{m,n}^+(x) - M_x\left(1 - \alpha_{m,n}^2\right)}{1 - \alpha_{m,n}^2 M_x^2} \tag{13}$$

### C. Equivalence of the Spinning Mode Amplitude Minimization Objective with Pressure Minimization

It is straightforward to show that if the mode amplitudes are uniformly weighted, $w_m = 1$, then the control performance achieved using the modal control objective of Eq. (9) is identical to that obtained in the case of pressure minimization of Eq. (8). This can be shown by examining the pressure at the $l$th error sensor position, which can be expressed as the sum of the spinning mode amplitudes $\hat{a}_m$ at the duct wall:

$$p(\theta_l) = \sum_{m=-m_{\max}}^{m_{\max}} \hat{a}_m e^{im\theta_l} \tag{14}$$

where $m_{\max}$ is the highest spinning mode order with a significant amplitude at the error sensor array. Each spinning mode amplitude $\hat{a}_m$ comprises the sum of radial modes:

$$\hat{a}_m = \sum_{n=1}^{\infty} a_{m,n} \Psi_{m,n}(a) \tag{15}$$

Assuming $L$ error sensors, the amplitudes of the spinning modes after control can be obtained by performing the spatial discrete Fourier transform (DFT) of the pressure measurements at the duct wall,

$$\hat{a}_m = \frac{1}{L} \sum_{l=1}^{L} p(\theta_l) e^{-im\theta_l} \qquad \left[ \frac{-(L-1)}{2} \le m \le \frac{L-1}{2} \right] \tag{16}$$

If the pressures are driven to zero at the error sensors,

$$p(\theta_l) = 0 \qquad (1 \le l \le L) \tag{17}$$

and the number of sensors exceeds the number required to satisfy the Nyquist criterion of $L \ge 2|m_{\max}| + 1$, then Eq. (17) indicates that the individual spinning mode orders will also be driven to zero, that is,

$$\hat{a}_m = 0 \qquad [-(L-1)/2 \le m \le (L-1)/2] \tag{18}$$

Essentially therefore, if a sufficient number of sensors are used, the control system is decoupled in as much as the spinning mode amplitudes are independently driven to zero.

This relationship is reciprocal. Driving the sum of the spinning mode amplitudes at the duct wall to zero also drives the pressure at the error sensors to zero. This equivalence is only observed if the spinning mode amplitudes are uniformly weighted in the cost function of Eq. (9). We shall show in Sec. V that if the modes are weighted such that control is focused on the buzz-saw mode then, in the presence of noise, significant improvements in control performance can be achieved compared with when minimizing the sum of the squared pressures.

## IV. Control Performance with a Single Ring of Sources and Sensors

In all of the simulations presented here, 30 sources and sensors are assumed, arranged in a single ring as shown in Fig. 1. The use of this number of sources and sensors allows the detection and control of spinning mode orders up to $m = 14$ (Ref. 9). The fan plane is positioned at $x_f = 0.6$ m, the secondary sources are positioned at $x_s = 1$ m, and the error sensors at $x_e = 1.24$ m in a duct of length $L = 1.84$ m and a radius $a = 0.4$ m. The tip speed Mach number is $M_t = 1.05$ corresponding to an axial flow Mach number $M_x = -0.55$. The use of these values in Eq. (1) shows that, for

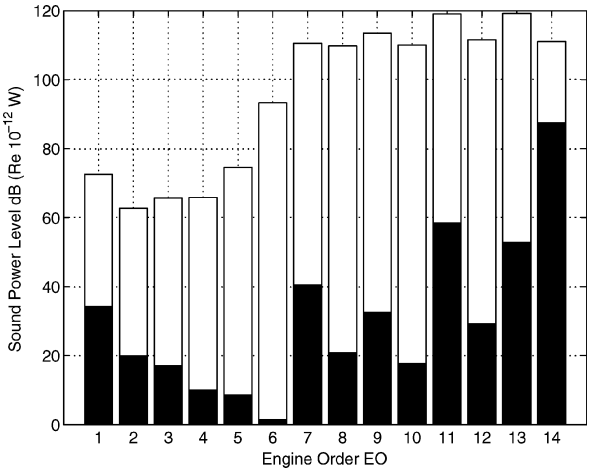


**Fig. 2 Sound power reduction for EO = 1–14 when minimizing the sum of the square pressures in the absence of noise or extraneous modes.**

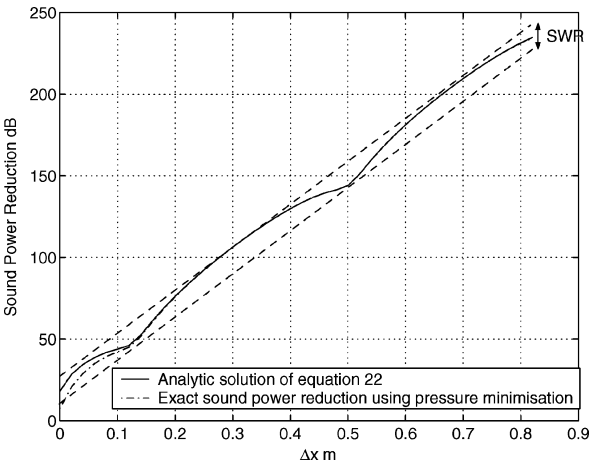


**Fig. 3 Sound power reduction for varying separation distance between sources and sensors obtained using the model of Eq. (22) and the exact calculation using 30 sources and sensors to control EO = 8. The departure from "straight-line" behavior is equal to the standing wave ratio of the buzz-saw noise field.**

EO = 1–14, only the first radial mode order can propagate, defined in this paper as $n = 1$.

Figure 2 shows the sound power reduction predicted for each EO when minimizing the sum of the square pressures (and modal control for $w_m = 1$). The white bars show the sound power level before control, and the solid bars show the resulting levels after control. The values of $a_{p_0}$ at each frequency were determined using the FDNS method developed by McAlpine and Fisher[10] using estimated data for the sound pressure levels at the fan face.

The sound power reduction increases from EO = 1 to 5. At this tip speed these buzz-saw modes are cut off; however, the control system is unable to identify them as evanescent modes, and thus the control system will attempt to control these cutoff EO. The buzz-saw mode at EO = 5 is the closest to cut on (but still cut off) and will have decayed by the least amount by the time it reaches the error sensor array. Thus control performance will be greater than for the low EOs. At EO = 6–13, sound power reductions of between 70 to 90 dB are obtained in this noise-free simulation. However, at EO = 14, the sound power is reduced by only 10–15 dB. This is because at this frequency the sources inadvertently excite the $m = -16$ mode, which is only just cut off. (The 30 sources and sensors cannot independently control modes $m \geq 15$.) Modal spillover as a result of aliasing of high spinning mode components at these high EOs will therefore considerably limit control performance, as observed in Fig. 2. This phenomenon can be explained using the Nyquist sampling relationships discussed in Sec. III.C.

The control performance of the active control system is now discussed in detail for the representative frequency of EO = 8 ($m_B = 8$, $n = 1$).

### A. Effect of Source/Sensor Array Separation Distance on Active Control Performance

The model described in Sec. II was used to predict the variation in sound power reduction with separation distance $\Delta x = x_e - x_s$ between the source and sensor rings. The results are plotted in Fig. 3 at EO = 8 for 30 sources and sensors.

Figure 3 shows that control performance improves dramatically with increasing separation distance $\Delta x$ at a rate of approximately 250 dBm$^{-1}$ in this example. It can also be seen that the sound power reduction dips at approximately $\Delta x = 0.1$ and 0.5 m. These positions correspond to error sensor positions situated at the minima of the primary field standing wave field set up between the reflective terminations (assuming no blockage by the rotor and stator). When the sensors are positioned at these points, the coupling between sources and sensors is comparatively weak. We shall later show that control performance at these positions is predicted to be reduced by an amount no greater than half of the standing wave ratio of the primary buzz-saw field.

Figure 4 shows the mode amplitudes and mode powers after minimization of the sum of the squared pressures. (Identical results are

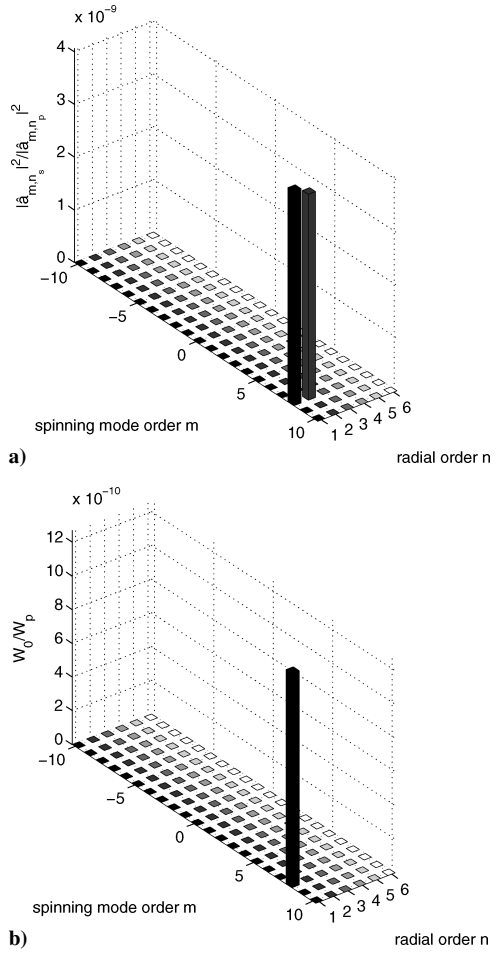


**Fig. 4 Minimization of the sum of the squared pressures: a) modal pressure amplitudes at the sensor array after minimization of the sum of the squared pressures and b) modal power at the sensor array after minimization of the sum of the squared pressures.**

observed when minimizing the sum of the squared spinning mode amplitudes.) In the process of controlling the propagating buzz-saw mode (8,1), the secondary sources are also observed to excite the second radial mode $n = 2$ associated with the $m = 8$ mode, which is cut off. The pressure at the error sensors after control is close to zero (−300 dB). To achieve this level of pressure reduction, therefore, the modes (8,1) and (8,2) are excited such that they destructively interfere at the error sensors. However, the propagating mode (8,1)

carries substantially more power than the evanescent (8,2) mode. Thus the level of the sound power reduction achievable by pressure minimization will be determined by the pressure of this evanescent mode at the error sensor array. At small separation distances the level of the evanescent mode is comparatively high, and hence the power reduction is comparatively small. As the separation distance increases, the modal decay increases, and the sound power reduction increases.

### B. Analytic Model for the Prediction of Sound Power Reduction by Pressure Minimization

Based on the control mechanism just discussed, a simple analytic model is now developed, which predicts the control performance characteristics illustrated in Fig. 3. The model makes the following simplifying assumptions:

1) The secondary source ring will only excite radial modes at $m = m_B$, including evanescent modes. This assumption is valid provided that sufficient sources and sensors are confined to a single ring.

2) There are at least as many sensors as sources so that the pressure is driven exactly to zero at the error sensors. This is a valid assumption as the overall pressure after control is typically in excess of 100 dB below that of the primary pressure in this noise-free simulation.

Setting the total pressure at the $l$th error sensor to zero gives

$$p(\theta_l, x_e) = \left[a_{p_{m_B,1}}(x_e) + a_{s_{m_B,1}}(x_e)\right]\Psi_{m_B,1}(a)e^{im_B\theta_l} + \sum_{n=2}^{\infty}\left[a_{p_{m_B,n}}(x_e) + a_{s_{m_B,n}}(x_e)\right]\Psi_{m_B,n}(a)e^{im_B\theta_l} = 0 \tag{19}$$

where the primary $a_{p_{m,n}}$ and secondary $a_{s_{m,n}}$ modal amplitudes have been split into their propagating modes $(m_B, 1)$ and evanescent modes $(m_B, n > 1)$. In the case of the primary sound field, the distance between the fan and the error sensors is generally much greater than the distance between the secondary sources and the error sensors. The level of the evanescent modes from the primary source can therefore be neglected in this analysis. Equation (19) can be rearranged to obtain the following expression for the buzz-saw mode amplitude after control:

$$a_{m_B,1}(x_e) = a_{p_{m_B,1}}(x_e) + a_{s_{m_B,1}}(x_e) = -\frac{\sum_{n=2}^{\infty} a_{s_{m_B,n}}(x_e)\Psi_{m_B,n}(a)}{\Psi_{m_B,1}(a)} \tag{20}$$

which involves only evanescent modes $(n > 1)$.

Assuming that the power carried by the evanescent modes can be neglected, the maximum theoretical sound power reduction after control can be calculated from Eqs. (11) and (20) to give

$$\frac{W_0(x_e)}{W_p(x_e)} = \frac{\gamma_{m_B,1}(x_e)\left|a_{m_B,1}(x_e)\right|^2}{\gamma_{m_B,1}(x_e)\left|a_{p_{m_B,1}}(x_e)\right|^2} = \frac{\left|\sum_{n=2}^{\infty} a_{m_B,n}(x_e)\Psi_{m_B,n}(a)\right|^2}{\left|a_{p_{m_B,1}}(x_e)\Psi_{m_B,1}(a)\right|^2} \tag{21}$$

Further assuming that the most dominant cutoff mode is the $n = 2$ mode, the sound power level reduction $\Delta SWL = -10\log_{10}(W_p/W_0)$ in decibels can be written as

$$\Delta SWL(x_e) = \overbrace{\Delta SWL(x_s)}^{1} - \overbrace{8.7\,\mathrm{Im}\left\{k_{x_{m_B,2}}\right\}(x_e - x_s)}^{2} + \overbrace{10\log\left|\frac{\cos^2\phi^+_{m_B,1}(x_e)}{\cos^2\phi^+_{m_B,1}(x_f)}\right|}^{3} \tag{22}$$

The three terms in Eq. (22) completely describe the characteristics observed in Fig. 3, which can be interpreted as follows:

1) Term 1 is equal to the sound power reduction at zero separation distance between the sources and sensors (i.e., the $y$ intercept in Fig. 3).

2) Term 2 is the dominant term in the equation and describes the overall decay rate of the sound power attenuation with $\Delta x$. It is identically equal to the decay rate of the evanescent radial mode $(m_B, 2)$.

3) Term 3 is an oscillatory function and describes the departure from the straight line behavior observed in Fig. 3. The dips in Fig. 3 coincide with the minimum values of the function. Comparison of this term with Eq. (6) shows that it is related entirely to the standing wave behavior of the primary field. As demonstrated in Fig. 3, the maximum variation in power reduction from straight-line behavior is identical to the standing-wave ratio of the buzz-saw noise field.

The solid line in Fig. 3 is the sound power reduction predicted by Eq. (22). Excellent agreement is shown between the exact solution and this analytical model for separation distances greater than 0.1 m. Below this separation distance the assumption that the second radial mode is the most significant evanescent mode breaks down and Eq. (22) incorrectly predicts the sound power reduction.

### C. Control Performance vs Engine Speed

It was shown in Sec. II that at frequencies close to the cutoff frequency of the buzz-saw mode the modal reflection coefficients at both ends of the duct are close to unity. To assess how control performance varies as the fan tip speed is reduced, so that the frequency is taken through cut off, predictions were made over the frequency range around cut off. Figure 5 shows the sound power of the sound field at EO = 8 vs the tip speed Mach number, before and after control, following minimization of the sum of squared pressures (again assuming that $M_x = -0.52\,M_t$). In plotting the performance predictions against blade tip Mach number and buzz-saw mode cutoff ratio, the results are generalized to any size of engine duct. It is therefore anticipated that active control performance on any sized engine duct will be approximately similar for the same tip speed Mach number (or modal cutoff ratio).

The sound power "spectrum" of the primary buzz-saw field (solid curve) contains a series of resonant peaks caused by axial standing waves between the duct terminations. As the frequency is increased above cutoff, the resonance bandwidths become broader. This is because as the frequency (fan speed) increases the reflection coefficients decrease, leading to increasingly damped resonances through radiation damping. The frequencies (and hence the values of $\zeta$) of these resonant peaks are determined by setting the real part of the denominator of Eq. (6) equal to zero.

After control (dashed curve) the resonant peak frequencies become markedly shifted. A new set of axial standing wave regions have been created as a consequence of the control process. The analytical approach used in the preceding section can be used to predict the frequencies of these new resonances. From Eqs. (11) and (19),

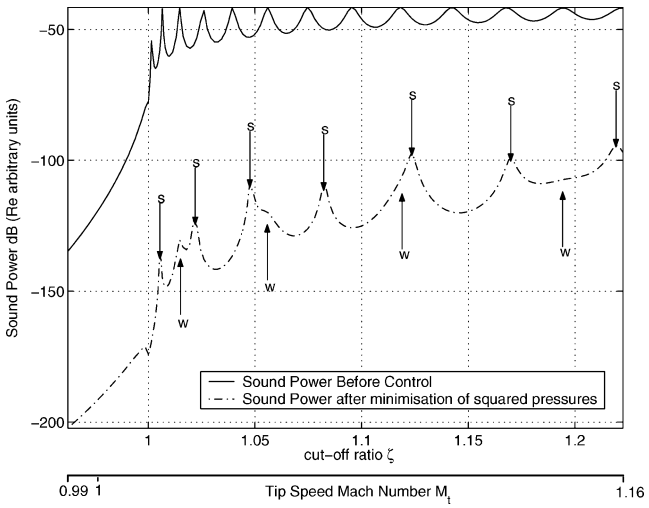


**Fig. 5 Active control performance with varying tip speed for a single ring of 30 sources and 30 sensors at EO = 8. The arrows indicate the family of strong (s) and weak (w) resonances after control.**

the sound power after control is given by

$$W_0(x_e) = \gamma_{m_B,1}(x_e)\left|\frac{a_{m_B,2}(x_e)\Psi_{m_B,2}(a)}{\Psi_{m_B,1}(a)}\right|^2 \tag{23}$$

The amplitude of the evanescent mode $a_{m_B,2}$ appearing in Eq. (26) can be deduced by summing the pressure contributions from $J$ secondary sources at position $\theta_{s_j}(j=1,2\ldots,J)$. It can be written as the product of a modal source strength $Q_{m_B}$ and a modal transfer impedance $z_{m_B,2}$ between the source and sensor, that is, $a_{m_B,2}(x_e) = Q_{m_B} z_{m_B,2}(x_s, x_e)$, where $Q_{m_B}$ is the $m_B$th harmonic spatial component of the secondary source ring defined by

$$Q_{m_B} = \sum_{j=1}^{J} q\left(x_{s_j}, r_{s_j}, \theta_{s_j}\right) e^{-im_B\theta_{s_j}} \tag{24}$$

The spinning mode transfer impedance $z_{m_B,2}(x_s, x_e)$, which describes how the modal source strength $Q_{m_B}$ couples into a specific mode at the error sensor plane, is derived from Eq. (2) and can be written for any mode $(m,n)$ as

$$z_{m,n}(x_s, x_e) = \frac{i\rho c_0 \Psi^*_{m,n}(a)}{S\alpha_{m_B,n}\left[\tan\phi^+_{m,n}(x_s) - \tan\phi^-_{m,n}(x_s)\right]} \times \frac{\cos\phi^+_{m,n}(x_e)}{\cos\phi^+_{m,n}(x_s)} \exp\left[\frac{-ikM_x(x_e - x_s)}{1-M_x^2}\right] \tag{25}$$

By expressing the secondary amplitudes in Eq. (19) in terms of the modal source strength $Q_{m_B}$ of Eq. (24), the expression for the modal source strength that drives the pressure to zero at the $l$th error sensor is of the form,

$$Q_{m_B} = \frac{-a_{p_{m_B,1}}(x_e)\Psi_{m_B,1}(a)}{z_{m_B,1}(x_s, x_e)\Psi_{m_B,1}(a) + z_{m_B,2}(x_s, x_e)\Psi_{m_B,2}(a)} \tag{26}$$

Substituting Eq. (26) and Eq. (25) into Eq. (23) yields an expression for the sound power after control, which in nondimensional form is given by

$$\frac{W_0}{S/\rho c_0\left|a_{p_0}\right|^2} = \frac{S\gamma_{m_B,1}(x_e)\left|z_{m_B,2}(x_s, x_e)\Psi_{m_B,2}(a)\right|^2}{\rho c_0|\Psi_{m,n}(a)|^2}\left|\alpha_{m_B,1}\right|^2 \times \frac{\left|e^{i\phi^-_{m_B,1}(x_f)}\right|^2}{\left|\cos\phi^-_{m_B,1}(x_s)\right|^2} \tag{27}$$

Equation (27) reveals two independent families of resonances in the spectrum of sound power after control.

The first class of resonances is the strongest (marked s in Fig. 5) and is produced as a consequence of standing waves between the secondary sources and the exhaust termination. These can be explained by the following control process:

1) At a time $t=0$ the buzz-saw mode "reaches" the source array (at position $x_s$), where the control system generates a mode of equal amplitude but in antiphase. However, the secondary source radiates in both directions along the duct.

2) The forward wave partially cancels with the buzz-saw mode as the sources attempt to control both the buzz-saw mode and the first cutoff mode. However, the backward-propagating mode is unattenuated.

3) At $t = 2x_s/c_0$ (neglecting convection effects) the reflected secondary wave arrives back at the source array, and the sources will radiate a mode to attenute the reflection. This will cancel with the forward wave; however, once again a mode is launched toward the exhaust termination, which is unattenuated.

4) This process continues indefinitely to create standing waves between the sources and the exhaust termination. At certain frequencies $\omega_q$ $(q=-\infty\ldots\infty)$ the in-duct pressure is continually being reinforced to produce axial resonances.

The frequency of these "strong" resonances occurs when the denominator term in Eq. (27) $|\cos\phi^-_{m_B,1}(x_s)|^2$ takes minimum values, that is, when

$$\mathrm{Re}\left[\phi^-_{m_B,1}(x_s)\right] = \mathrm{Re}\left[\frac{\ell_n R^-_{m_B,1}(\omega)}{2i} + \frac{\alpha_{m_B,1}k_q(-x_s)}{1-M_x^2}\right] = (2q+1)\frac{\pi}{2} \tag{28}$$

where $\omega_q = ck_q$. Solutions of Eq. (28) for the strong resonant peaks are marked with an s in Fig. 5.

However, Eq. (28) does not predict all of the resonances seen in Fig. 5 An additional class of "weaker" resonances is also present after control, which is most easily seen at low-fan-tip-speed Mach number.

These weaker resonances (marked w in Fig. 5) are associated with minima in the denominator of the $\gamma_{m_b,1}(x_e)$ power function, which from Eq. (11) and Eq. (13) is $\cos\phi^+_{m_B,1}(x_e)$. From Eq. (4) this resonance condition occurs when $\mathrm{Re}\{\cos[\phi^+_{m_B,1}(x_e)]\} = 0$, that is, when

$$\mathrm{Re}\left[\phi^+_{m_B,1}(x_e)\right] = \mathrm{Re}\left[\frac{\ell_n R^+_{m_B,1}}{2i} + \frac{\alpha_{mn}k_q(L-x_e)}{1-M_x^2}\right] = (2q+1)\frac{\pi}{2} \tag{29}$$

Equation (29) defines axial resonances over the distance $(L-x_e)$, which is the distance between the sensor array and the inlet termination. The frequency solutions of Eq. (29) for these weaker resonances are marked on Fig. 5 with a w.

These can be explained by examining the control mechanism forward of the fan, as described next:

1) The forward-going wave is only partially canceled because of the presence of the evanescent radial mode at the error sensor array and the residual wave travels toward the inlet termination.

2) After a time $t = (2L - x_e - x_s)/c_0$ (neglecting convection effects), the residual reflected propagating mode will reach the sensor array. The secondary sources anticipate its arrival and launch a wave at time $t = 2(L-x_e)/c_0$ to attenuate it further.

3) The launched wave will once again be an underestimate of the buzz-saw mode amplitude, and thus this process will continue indefinitely setting up a standing wave between the sensors and the inlet termination. At certain frequencies $w_q$ therefore, axial resonances are produced.

## V. Active Control Performance in Presence of Extraneous Modes and Noise at Error Sensors

Throughout the preceding sections, it has been assumed that only a single propagating mode exists at each engine order in the primary buzz-saw sound field. Hence, unrealistically large sound power reductions are predicted. The study is useful, however, for illustrating the principles of active noise control for controlling buzz-saw tones. In reality, there will be both extraneous modes in the primary field and locally generated noise at the error sensor array. To examine their effects on control performance, simulation results are now presented in which extraneous modes comprising all of the propagating modes are assumed to be present at each engine order of interest. Also presented in this section is the predicted control performance where the noise is caused solely by local noise at the error sensor array.

### A. Control Performance in the Presence of Extraneous Modes in the Primary Field

In this section, the noise at the error sensors is assumed to be solely caused by extraneous modes. Here all propagating modes are assumed to be present with equal amplitude $a_{\mathrm{em}}$, as determined from the signal-to-noise ratio defined here by $\mathrm{SNR}_{\mathrm{em}} = -20\log_{10}(N|a_{\mathrm{em}}|/|a_{m_B,1}|)$, where $N$ is the number of propagating modes. The phase of the modal amplitudes is chosen here at random with the performance predictions obtained from a single realization. Control performance with varying tip speed of the three different control objectives obtained using a single ring of 30 sources and a single ring of 30 sensors at EO = 8 with $\mathrm{SNR}_{\mathrm{em}} = 20$ dB is shown in Fig. 6. These predictions represent a

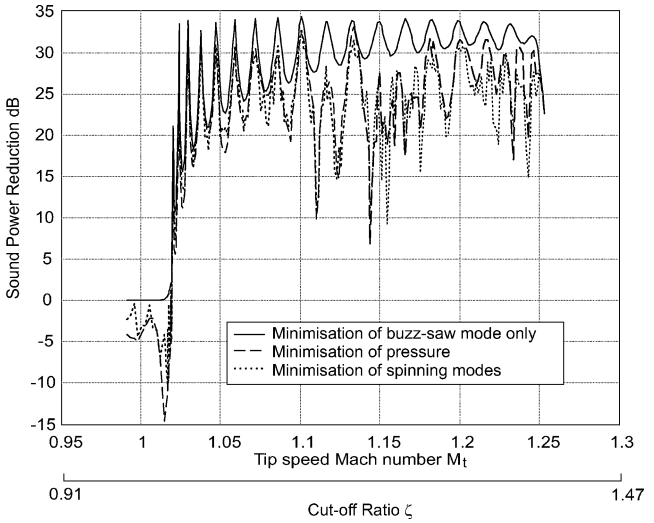


**Fig. 6 Active control performance with varying tip speed for a single ring of 30 sources and 30 sensors and with extraneous modes at the fan face at levels 20 dB below the level of the buzz-saw mode.**

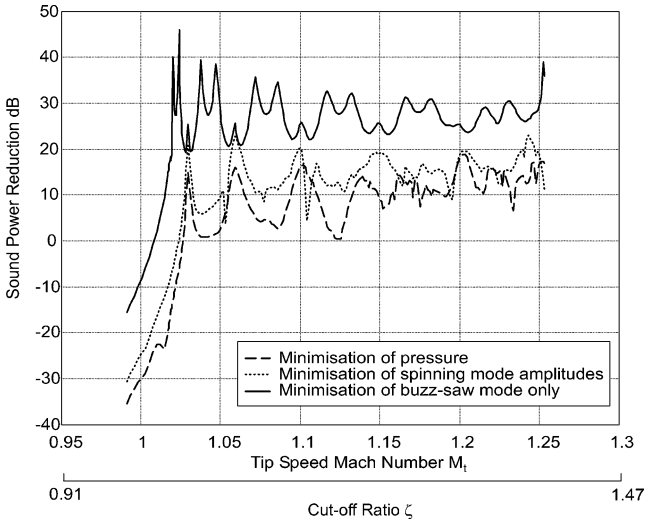


**Fig. 7 Active control performance with varying tip speed for a single ring of 30 sources and 30 sensors and with local noise at the error sensors at a level 20 dB below the level of the buzz-saw mode.**

pessimistic estimate of control performance as recent modal analysis buzz-saw noise measurements indicate extraneous mode levels lower than that assumed here.

In the presence of extraneous modes, control performance obtained following pressure minimization and spinning mode amplitude minimization for $w_m = 1$ objectives becomes significantly degraded compared to the reduction observed in Fig. 5, with extraneous modes absent. At low tip speeds, power reductions of approximately 30 dB are obtained. At higher tip speeds the reduction is less. In the presence of extraneous modes, the number of sources and sensors in this simulation are sufficient to detect and control all propagating modes. In both the pressure minimization and uniformly weighted spinning mode amplitude case, therefore, both the pressure at the error sensors and the spinning mode amplitudes at the duct wall are driven to zero. Similar sound power reductions are therefore obtained. At low spinning mode orders $m$, multiple radial mode orders can propagate in the duct. However, the single-ring control system cannot resolve these radial mode orders. For the spinning mode amplitudes to be driven to zero, therefore, the secondary source array excites the radial modes such that they destructively interfere, but at the expense of increasing their amplitudes. This results in an increase in the sound power carried by the extraneous modes after control.

In the case in which control is focused on the buzz-saw mode (solid line), therefore, control occurs solely in the mode order $m = m_B$. The control principle described in Sec. IV applies in this case where the propagating buzz-saw mode is equal to the second evanscent radial mode after control. Figure 6 shows that sound power reductions of up to 35 dB are observed for all tip speeds. This control strategy is therefore more effective when the dominant "noise" source is from extraneous modes.

### B. Active Control Performance in the Presence of Locally Generated Noise at the Error Sensors

The second type of noise that could be present at the error sensors is that of "local" noise. This noise is generally not modal in structure and can be caused by flow noise generated locally at the microphones. Here, the noise is defined in terms of a signal-to-noise ratio of the amplitude of the noise $n_p$ to the amplitude of the primary pressure at a single sensor, $\mathrm{SNR}_{\ell n} = 20\ \log_{10}(|p_p(\theta_l)|/|n_p|)$. The phase of the noise signal at each error sensor was once again chosen at random. The noise signals are added to the primary pressure measured at the error sensors, $p_{p_n}(\theta_l) = p_p(\theta_l) + n_p(\theta_l)$.

Active control performance predicted in the presence of local noise for all three control objectives is plotted in Fig. 7 against tip speed for the control system with 30 sources and 30 sensors at EO = 8 with $\mathrm{SNR}_{\ell n} = 20$ dB.

Control performance in this case is significantly better than that predicted in the presence of extraneous modes for the same signal-to-noise ratio. Noise local to the error sensors will be "observed" as effectively having contributions from all spinning mode orders $m$. Every mode therefore has a significant amplitude at the error sensor array. There are insufficient sources and sensors to detect and control all modes in this case, and hence the pressure is not driven to zero. This in turn suggests that the extraneous modes excited by the secondary sources are not driven to destructively interfere. Thus the sound power reduction is greater than in the extraneous mode case for the same SNR. Once again, significant improvements in sound power reduction of typically 15 dB can be achieved at some tip speeds by confining control to the buzz-saw mode.

## VI. Conclusions

This paper has shown that buzz-saw noise can be substantially attenuated using an active noise control system comprising a single ring of sources and sensors when there are no extraneous modes or noise present.

In the absence of extraneous modes and noise at the error sensors, it has been shown that the level of evanescent modes excited by the secondary sources measured at the error sensor array fundamentally limits the sound power reduction possible when the sum of the squared pressures is minimized or equivalently. Following the minimization of the sum of the squared pressures at the error sensors using a single ring of sources, strong standing waves are set up between the exhaust termination and the source array and much weaker standing waves between the sensors and the inlet termination.

The control mechanism has been examined with respect to the spatial DFT relationship between the error sensors and the spinning mode amplitudes at the duct wall. This relationship was used to show that the minimization of the sum of the squared pressures and the minimization of the sum of the squared amplitudes at the duct walls will yield identical control performance. In the presence of extraneous modes and noise at the error sensors, it has been shown that control performance is significantly improved by weighting the cost function such that control is focused on the buzz-saw mode.

## Acknowledgment

The research presented in this paper is funded by the European Union SILENCE(R) project.

## References

[1]McAlpine, A., Fisher, M. J., and Tester, B. J., "'Buzz-Saw' Noise: A Comparison of Measurement with Prediction," *Journal of Sound and Vibration*, Vol. 290, Nos. 3–5, 2006, pp. 1202–1233.

[2]Smith, J., and Burdisso, R., "Active Control of Inlet Noise from a Turbofan Engine Using Inlet Wavenumber Sensors," *Proceedings of the 5th AIAA/CEAS Conference*, AIAA, Reston, VA, 1999, pp. 66–76.

[3]Kousen, K. A., and Verdon, J. M., "Active Control of Wake Blade-Row Interaction Noise," *AIAA Journal*, Vol. 32, No. 10, pp. 1953–1960.

[4]Joseph, P., Nelson, P., and Fisher, M., "Active Control of Fan Tones Radiated from Turbofan Engines I. External Error Sensors," *Journal of the Acoustical Society of America*, Vol. 106, No. 2, 1999, pp. 766–78.

[5]Joseph, P., Nelson, P., and Fisher, M., "Active Control of Fan Tones Radiated from Turbofan Engines II. In-Duct Error Sensors," *Journal of the Acoustical Society of America*, Vol. 106, No. 2, 1999, pp. 779–786.

[6]Kraft, R., and Kontos, K., "Theoretical Implications of Active Noise Control for Turbofan Engines," *15th AIAA Aeroacoustics Conference*, AIAA, Washington, DC, 1993.

[7]Risi, J., Burdisso, R. A., and Fuller, C. R., "Analytical Investigation of Active Control of Radiated Inlet Fan Noise," *Journal of the Acoustical Society of America*, Vol. 99, No. 1, 1996, pp. 408–416.

[8]Fruteau, E., Joseph, P., and Nelson, P., "Final Report on the Reduction of Aircraft Noise by Nacelle Treatment and Active Control (RANNTAC)," Inst. of Sound and Vibration Research, Tech. Rept. 00/36, Univ. of Southampton, Southampton, England, U.K., Dec. 2000.

[9]Wilkinson, M. J., Joseph, P. F., and McAlpine, A., "Active Control of Buzz-Saw Tones," *ACTIVE 2002*, edited by P. Gardonio and B. Rafaely, Inst. of Sound and Vibration Research, Univ. of Southampton, Southampton, England, U.K., 2002, pp. 588–601.

[10]McAlpine, A., and Fisher, M. J., "On the Prediction of 'Buzz-Saw' Noise in Aero-Engine Inlet Ducts," *Journal of Sound and Vibration*, Vol. 248, No. 1, 2001, pp. 123–149.

[11]Morfey, C. L., "Sound Transmission and Generation in Ducts with Flow," *Journal of Sound and Vibration*, Vol. 14, No. 1, 1971, pp. 37–55.

[12]Wilkinson, M., "Active Control of Low Frequency Buzz-Saw Tones," Ph.D. Dissertation, Inst. of Sound and Vibration Research, Univ. of Southampton, Southampton, England, U.K., Dec. 2004.

[13]Mugridge, B. D., and Morfey, C. L., "Sources of Noise in Axial Flow Fans," *Journal of the Acoustical Society of America*, Vol. 51, No. 5, Pt. 1, 1972, pp. 1411–1426.

[14]Zorumski, W. E.,"Generalized Radiation Impedances and Reflection Coefficients of Circular and Annular Ducts," *Journal of the Acoustical Society of America*, Vol. 54, No. 6, 1973, pp. 1667–1673.

[15]Johnston, G. W., and Ogimoto, K., "Sound Radiation from a Finite Length Unflanged Circular Duct with Uniform Axial Flow 1. Theoretical Analysis," *Journal of the Acoustical Society of America*, Vol. 68, No. 6, 1980, pp. 1858–1870.

B. Balachandran
*Associate Editor*